

## Femtosecond Photoelectron Imaging of N<sub>2</sub> at 410 nm

Wei Guo,<sup>\*</sup> Shanshan Wei, Xingqiang Lu,<sup>†</sup> and Li Wang<sup>‡</sup>

School of Electric Engineering, University of South China, Hengyang 421001, P. R. China. \*E-mail: wei.guo@chem.queensu.ca

<sup>†</sup>School of Nuclear Science and Technology, University of South China, Hengyang 421001, P. R. China

<sup>‡</sup>State Key Laboratory of Molecular Reaction Dynamics, Dalian Institute of Chemical Physics, Dalian 116023, P. R. China

Received June 27, 2010, Accepted October 11, 2010

We experimentally measure the kinetic energy and angular distributions of photoelectrons of N<sub>2</sub> as a function of 410 nm femtosecond laser intensity by using velocity map imaging technique. The strong-field multiphoton ionization of molecules shares many of the characteristics with those of atoms. Electron kinetic energies are nearly independent of laser intensities. The independence suggests that the electron peaks in the photoelectron spectrum actually result from a two-step process, indicative of the occurrence of real population in the intermediate states. The relative amplitudes of electron peaks indicate that in the two-step process, nonresonant population transfer dominates for low intensities, while resonant population transfer dominates for higher intensities.

**Key Words:** Two-step model, Rydberg states, Ponderomotive potential, Resonant/nonresonant population transfer

### Introduction

The multiphoton ionization (MPI) dynamics of molecules in intense laser fields has received numerous experimental and theoretical researches.<sup>1–6</sup> It is considerably more complicated compared to atoms due to their multicenter nature, which introduces additional vibrational and rotational degrees of freedom, and a detailed understanding of the ionization mechanism remains unsettled. A powerful approach in studying the dynamic processes is using velocity map imaging where simultaneous measurement of the photoelectron kinetic energy and angular distributions facilitates the identification and classification of ionization mechanisms.<sup>7,8</sup> The photoelectron energy spectra and angular distributions often reflect the nature of the dominant intermediate states, and are important for an understanding of strong-field molecular physics.

The narrow peaks in the short-pulse regime photoelectron spectrum of atoms in strong fields have been interpreted by two types of mechanisms: the resonant enhancement model<sup>9–12</sup> and the two-step model.<sup>13</sup> For the former mechanism, the electron peaks result from an enhancement of the MPI rate brought about by the ac Stark effect of excited states into resonance with the laser field at the peak of the laser pulse. Therefore electrons born at different laser intensities appear at different electron kinetic energies. For the latter mechanism, first an intermediate state is ac Stark shifted into resonance and populated. Subsequently, a fraction of the excited molecules is ionized. Therefore, the kinetic energy of all electrons ionized out of the same state is independent of the ionizing intensity. The two pictures have been used to successfully model experimental results for atoms.<sup>10–15</sup> Previous studies provide evidence that strong-field ionization of molecules shares many of the characteristics with those of atoms,<sup>1,2</sup> and indeed the two mechanisms have been observed by previous experimental results for molecules.<sup>1–3</sup>

N<sub>2</sub> is one of the two major ingredients of the atmosphere, and its MPI dynamics in intense femtosecond laser fields has

been studied extensively. Gibson *et al.* suggested that Rydberg states act as intermediates at high intensities, and N<sub>2</sub><sup>+</sup> B<sup>2Σ<sub>u</sub><sup>+</sup> dominated at 308 nm, while all the ionization channels (X<sup>2Σ<sub>g</sub><sup>+</sup>, A<sup>2Π<sub>u</sub><sup>+</sup>, and B<sup>2Σ<sub>u</sub><sup>+</sup>) were significant at 616 nm by using conventional photoelectron spectroscopy. The difference originated from the difference between the ponderomotive potential  $U_p$  and the photon energy at a given laser intensity and a given wavelength.<sup>2</sup> Hu *et al.* simulated the experiment with time-dependent wavepacket method. Their calculations indicated that the three different ionic populations of N<sub>2</sub><sup>+</sup> (X<sup>2Σ<sub>g</sub><sup>+</sup>, A<sup>2Π<sub>u</sub><sup>+</sup>, and B<sup>2Σ<sub>u</sub><sup>+</sup>) increased with intensities, but the ionic population of N<sub>2</sub><sup>+</sup> B<sup>2Σ<sub>u</sub><sup>+</sup> increased more quickly than the other two ionic populations, leading to the larger population at 308 nm.<sup>4</sup> Chu *et al.* and Dundas *et al.* suggested that at lower laser intensities, where only one type of electrons, the electrons in the highest occupied molecular orbital (HOMO), are most active, whereas at higher intensities, different inner valence electrons corresponding to different molecular orientations ionize significantly.<sup>5,6</sup> Tsubouchi *et al.* numerically simulated the axis alignment and photoionization of N<sub>2</sub> molecules. They suggested that the laboratory frame photoelectron angular distribution (LF PAD) expected for the ionization of laser-aligned molecules is largely similar to the molecular frame photoelectron angular distribution (MF PAD), though the LF PAD is typically a highly averaged quantity, and is significantly less structured than the MF PAD.<sup>16</sup></sup></sup></sup></sup></sup></sup></sup></sup>

In this paper, we report our experimental investigations on the photoelectron dynamics of N<sub>2</sub> in 70 fs, 410 nm laser field within the intensity order of 10<sup>14</sup> W/cm<sup>2</sup>, by using velocity map imaging technique.<sup>17</sup> Based upon the experimental results, the energy and angular distributions of photoelectrons in the MPI of N<sub>2</sub> are discussed.

### Experimental

The experimental setup has been described in detail else-

where.<sup>18</sup> Briefly, our homemade solid-state femtosecond laser system outputs 820 nm fundamental pulses (with ~20 nm bandwidth) at 20 Hz repetition rate with 70 fs width and 160 mW average powers. Pulse width is determined by single-shot intensity autocorrelation method. The fundamental light is frequency doubled by a  $\beta$ -BaB<sub>2</sub>O<sub>4</sub> crystal (BBO, type I) to produce second harmonic generation (SHG) light, centered at 410 nm.

The SHG beam is focused by a 30 cm fused quartz lens into the time-of-flight mass spectrometer (TOF-MS). The incident laser intensities can be varied by using different neutral density attenuators. The laser intensities at the focus spot are calibrated by the stark shifts in photoelectron energy spectra of Xe,<sup>9</sup> and are estimated to vary from  $1.28 \times 10^{14}$  W/cm<sup>2</sup> to  $2.88 \times 10^{14}$  W/cm<sup>2</sup> in our experiment. The laser polarization direction is perpendicular to the TOF axis.

The sample gas, 5% N<sub>2</sub> in He, is expanded through a pulsed valve (General Valve, with a 0.5 mm orifice) into the ionization accelerating region. The field-free region (40 cm) of the TOF was shielded with  $\mu$ -metal tube to avoid external magnetic fields that might otherwise deflect the electron trajectories. Electrons are detected by a two-stage microchannel plate (MCP) detector backed by a phosphor screen. Images on the screen are captured by a thermoelectrically cooled charge-coupled-device video camera (LAVISION Inc., Imager QE). Each image is the integral result over 20 000 laser shots. The emission from the phosphor screen is monitored by a photo-multiplier tube. Energy and angular distributions are obtained by Abel inversion of the raw images.<sup>19,20</sup> With the molecular beam on, the source chamber and flight chamber are maintained at  $4.5 \times 10^{-4}$  Pa and  $8 \times 10^{-6}$  Pa to avoid the space-charge effect.

## Results and Discussion

Figure 1 illustrates the typical experimental photoelectron images (left side) and inverted ones (right side) by Abel inver-

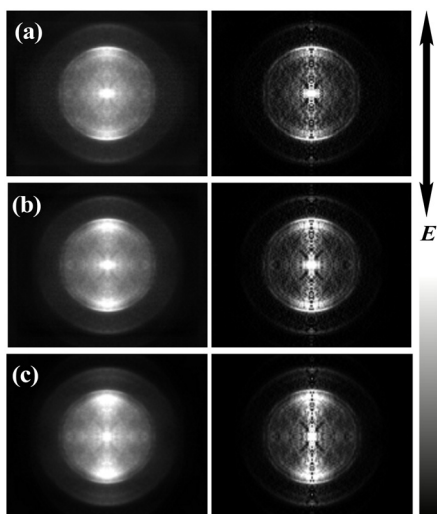


**Figure 1.** Raw experimental photoelectron images (left side) and inverted images (right side) of N<sub>2</sub> recorded at three laser intensities. (a)  $1.28 \times 10^{14}$  W/cm<sup>2</sup>. (b)  $1.92 \times 10^{14}$  W/cm<sup>2</sup>. (c)  $2.88 \times 10^{14}$  W/cm<sup>2</sup>. The vertical arrow and the gray bar represent the laser polarization and signal intensity, respectively.

sion at three different peak laser intensities. Two clusters of central rings are visible, and they are separated by the energy of one photon. The individual ring corresponds to photoelectrons with the same kinetic energies, and is characteristic for specific ionization channels.

Figure 2 shows the photoelectron kinetic energy distributions of N<sub>2</sub> for the intensity range of  $1.28 \times 10^{14}$ – $2.88 \times 10^{14}$  W/cm<sup>2</sup>. Each curve is normalized for better comparison of relative effects. The electron energy spectra are similar to that observed by Gibson *et al.* at an intensity of  $2.4 \times 10^{14}$  W/cm<sup>2</sup> for 308 nm, 150 fs laser pulse.<sup>2</sup> Despite the presence of extra molecular degrees of freedom, the MPI electron spectrum of N<sub>2</sub> in intense fields gives rise to very simple atomic-like photoelectron features. The simplicity occurs for two general reasons: First, in a short pulse, Rydberg states of resonance are the prominent feature of most photoelectron spectra. Second, the shifts of both the Rydberg states and the ionization threshold are approximately equal, and in conjunction with the propensity rule  $\Delta v = 0$ , where  $v$  is the vibrational quantum number, cancels out the vibration information in the photoelectron energy spectrum.<sup>1,2</sup>

The continuous, and decreasing electron energies for increasing laser intensity in the low kinetic energy range for 0 to 1 eV indicate nonresonant (NR) process,<sup>10,15</sup> as marked in Figure 2.

One phenomenon in Figure 2 is the location of four dominant photoelectron peaks (peaks at 1.57 eV, 1.81 eV, 2.17 eV, 4.76 eV, marked as 1, 2, 3, 4, respectively) is invariable with increasing laser intensities. The peak 4 is the first above-threshold ionization (ATI), corresponding to one additional photon absorption, i.e. 3.02 eV for 410 nm. The saturation of energy shift has been observed experimentally for the case of atoms in long-pulse regime.<sup>12</sup> It was suggested that the independence arises from the cancellation of the increased ionization energy

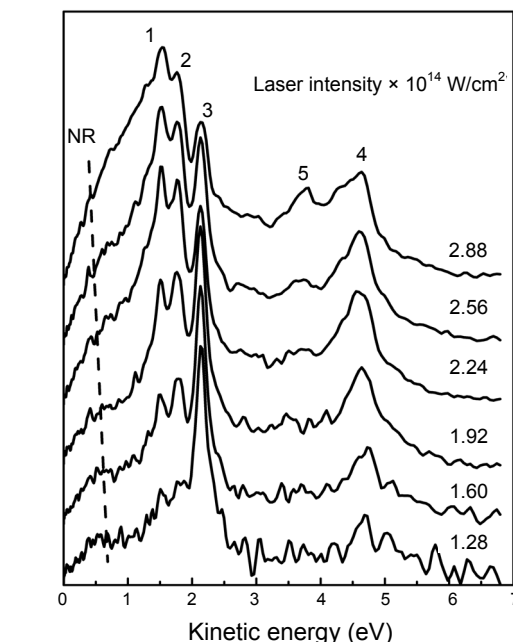


**Figure 2.** Photoelectron kinetic energy distributions of N<sub>2</sub> at various laser intensities. NR indicates nonresonant ionization process.

of the atom at the time of ionization, and the kinetic energy gained by the electron from ponderomotive acceleration as it leaves the focal region. Obviously, this is not the case in our experiment, since in short-pulse regime (in which the pulse duration of the laser is much shorter than the time taken by an electron to leave the laser focus, around 1 ps<sup>1</sup>) there is no time for the photoelectron to accelerate before the pulse leaves.<sup>13</sup>

Inconsistent with the generally accepted resonance enhancement model of short-pulse MPI: An intermediate state shifts into resonance at one specific value of the ac Stark shift and thereby at one intensity (resonant intensity),<sup>13</sup> the insensitivity of the photoelectron energy to laser intensities is an experimental signature of a two-step process: real population transfer and subsequent single- or multi-photon ionization. The key feature of this mechanism is that the excited-state population is ionized not only while that state is in resonance, but also it survives into the laser pulse and can be ionized at different laser intensities and different times throughout the laser pulse.<sup>13</sup> For a resonant ( $m + k$ ) MPI process, the electron kinetic energy is given by  $E_{\text{elec}} = khv - [I_p(0) - E(0)]$ , where  $I_p(0)$  and  $E(0)$  are, respectively, the ionization energy at zero field and zero-field energy of the resonantly intermediate state (assuming the ac Stark shift of the Rydberg state is equal to the ponderomotive potential  $U_p$ ).<sup>2,11</sup>

In  $N_2$  there are three different low-lying ionization energies (corresponding to the removal of the  $3\sigma_g$ ,  $1\pi_u$ , and  $2\sigma_u$  electrons) leading the ionic states  $X^2\Sigma_g^+$ ,  $A^2\Pi_u^+$ , and  $B^2\Sigma_u^+$ , respectively (simply, henceforth to be referred to as  $X$ ,  $A$ , and  $B$ ).<sup>2,5,6,21</sup> Given 410 nm photons (3.02 eV), a minimum of six-, six-, and seven-photons are necessary for ionization to  $X$  (15.58 eV),  $A$  (16.70 eV), and  $B$  (18.75 eV) ionic final states at zero fields, respectively. When the laser intensity is raised, the electrons acquire significant ponderomotive energy. Thus, to achieve ionization, more energy needs to be deposited in the system. Indeed, for intensities above  $9.05 \times 10^{13} \text{ W/cm}^2$  seven-photons need to be absorbed to bring the system into the  $A$  ionic final state. This particular intensity is referred to as the seven-photon ionization channel ( $A$ ) switching intensity.<sup>14</sup> In Figure 2 the peak 3 at 2.17 eV at  $1.92 \times 10^{14} \text{ W/cm}^2$  can be interpreted with

(6+1)-photon ionization via the  $(N_2^+ A) 4f, 4d\delta_g$  states (go through resonance at  $1.45 \times 10^{14} \text{ W/cm}^2$ ). In our experiment the energy resolution is, however, not sufficiently small to separate contributions from the  $(N_2^+ A) 4f$  and  $4d\delta_g$  states (energy separation of 10 meV<sup>22</sup>). Similar overlapping resonance has been reported on Xe<sup>9</sup> and Ar.<sup>14</sup> The corresponding angular distribution of peak 3 is shown in Figure 3. The angular distribution is obtained by integrating the concentric rings in the inverted image over a radius interval  $[r - dr, r + dr]$  ( $dr = 130 \text{ meV}$ ) at the azimuth angle from  $0^\circ$  and  $180^\circ$  in steps of  $1^\circ$  (the angle between the laser polarization and the electron velocity vector). No significant change in the angular distributions with peak intensity is observed for this ionization path (see Figure 3). The angular distribution displays four nodal planes in our experiment. Such a distribution is expected in ionization of a resonant intermediate state with aligned  $f(l=3)$  character because of the propensity in excitation of  $\Delta l = +1$  states.<sup>9,10,16</sup> This indicates a relatively strong contribution from the  $4f$  state. This state has been observed in a previous report on  $N_2$  by Gibson *et al.*, but they did not explore the angular information.<sup>2</sup>

Another phenomenon in figure 2 is the relative amplitudes of the first three peaks at different intensities. In the two-step model, for pulses whose peak intensities are higher than resonant intensity, the real population transfer consists of two parts: resonant population transfer at resonant intensity and nonresonant population transfer after resonant excitation during the pulse.<sup>13,23,24</sup> These two processes coexist and compete.<sup>23</sup> If the resonant population transfer dominates, one would expect a larger enhancement for peak 1, because this state requires greater intensities to be shifted into the resonance than peak 2 and peak 3 do, and thus relatively larger ionization rate at resonant intensity, leading to relatively larger amplitude of photoelectron peak 1.<sup>12</sup> It is clearly the case in our experiment for intensities above  $2.24 \times 10^{14} \text{ W/cm}^2$ . Traditionally, the resonant ionization signal increases with rising peak intensity due to volumetric growth.<sup>24,25</sup> If the nonresonant population transfer dominates, this should result in the larger enhancement for peak 3, because peak 3 requires lower intensities to be shifted into the resonance than peak 2 and peak 1 do, occurs on the

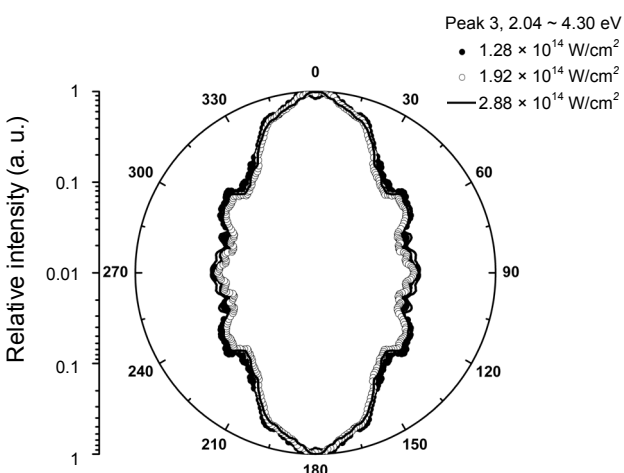


**Figure 3.** Photoelectron angular distribution of the peak 3 shown in Figure 2 at three different laser intensities.

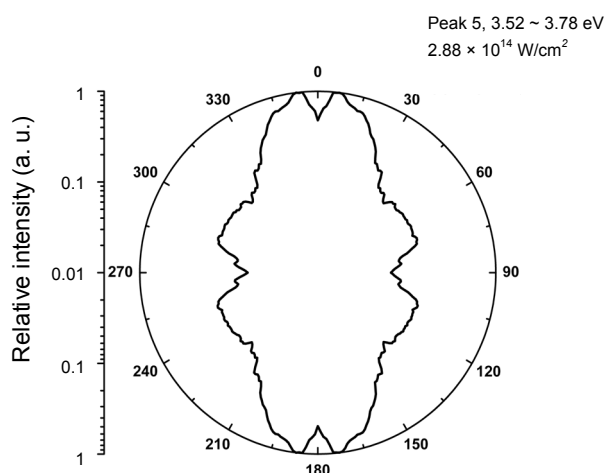


**Figure 4.** Photoelectron angular distribution of the peak 5 shown in Figure 2 at  $2.88 \times 10^{14} \text{ W/cm}^2$ .

early time of the pulse, and hence more nonresonant time, leading to relatively larger amplitudes of photoelectron peak 3. It is the case in our experiment for intensities below  $1.92 \times 10^{14} \text{ W/cm}^2$ . The nonresonant ionization signal increases with peak laser intensities because of the increasing nonresonant time.

The peak 5 at 3.65 eV is due to (5+2)-photon ionization via the  $(\text{N}_2^+ X) 3p\sigma_u$  Rydberg state. The corresponding angular distribution is shown in Figure 4. According to the rule: the orbital angular momentum changes by 1 for each photon absorbed, an additional minimum in electron intensity (a node) in the angular distribution is expected for the first ATI image.<sup>14,15</sup> The angular distribution of peak 5, as shown in Figure 4, displays three nodal planes (the signals around 0 and 180 degrees are noise produced from the Abel transformation), indicative of a resonant intermediate state with aligned  $p$  ( $l=1$ ) character, which agrees with our assignment of  $3p\sigma_u$  according to the kinetic energy. The absence of its corresponding non-ATI peak (i.e. (5+1)-photon ionization process, it should emerge at around 0.6 eV) is a signature of channel closure.<sup>26,27</sup> Because of the ponderomotive shift of the ionization threshold, above an intensity of  $1.62 \times 10^{14} \text{ W/cm}^2$  a minimum of seven-photon are required to ionize neutral  $\text{N}_2$  molecules and leave ions in  $\text{N}_2^+ X$  ionic final state, and the (5+1)-photon ionization channel via  $(\text{N}_2^+ X) 3p\sigma_u$  close off.

### Conclusion

The multiphoton ionization of  $\text{N}_2$  in intense femtosecond laser field for the intensity range of  $1\text{-}3 \times 10^{14} \text{ W/cm}^2$  at 410 nm has been studied experimentally by using velocity map imaging technique. The strong-field ionization of molecules shares many of the characteristics with those of atoms. The electron kinetic energies are nearly independent of the laser intensities. The independence suggests that the electron peaks in the photoelectron spectrum actually result from a two-step process, indicative of the occurrence of real population in the intermediate states. The relative amplitudes of electron peaks indicate that in the two-step process, nonresonant population transfer dominates for low intensities, while resonant population transfer dominants for higher intensities.

**Acknowledgments.** This work was supported by National Natural Science Foundation of China (Grants No. 20633070).

### References

1. Helm, H.; Dyer, M. J.; Bissantz, H. *Phys. Rev. Lett.* **1991**, *67*, 1234.
2. Gibson, G. N.; Freeman, R. R.; McIlrath, T. J. *Phys. Rev. Lett.* **1991**, *67*, 1230.
3. Lopez-Martens, R. B.; Schmidt, T. W.; Roberts, G. *Phys. Rev. A* **2000**, *62*, 013414.
4. Hu, J.; Meng, Q. T.; Han, K. L. *Chem. Phys. Lett.* **2004**, *393*, 393.
5. Chu, X.; Chu, S. I. *Phys. Rev. A* **2004**, *70*, 061402 (R).
6. Dundas, D.; Rost, J. M. *Phys. Rev. A* **2005**, *71*, 013421.
7. Parsons, B. F.; Sheehan, S. M.; Kautzman, K. E.; Yen, T. A.; Neumark, D. M. *J. Chem. Phys.* **2006**, *125*, 244301.
8. Plenge, J.; Nicolas, C.; Caster, A. G.; Ahmed, M.; Leone, S. R. *J. Chem. Phys.* **2006**, *125*, 133315.
9. Schyja, V.; Lang, T.; Helm, H. *Phys. Rev. A* **1998**, *57*, 3692.
10. Kaminski, P.; Wiehle, R.; Renard, V.; Kazmierczak, A.; Lavorel, B.; Faucher, O.; Witzel, B. *Phys. Rev. A* **2004**, *70*, 053413.
11. Gibson, G. N.; Freeman, R. R.; McIlrath, T. J. *Phys. Rev. Lett.* **1992**, *69*, 1904.
12. Freeman, R. R.; Bucksbaum, P. H.; Milchberg, H.; Darack, S.; Schumacher, D.; Geusic, M. E. *Phys. Rev. Lett.* **1987**, *59*, 1092.
13. De Boer, M. P.; Muller, H. G. *Phys. Rev. Lett.* **1992**, *68*, 2747.
14. Wiehle, R.; Witzel, B.; Helm, H.; Cormier, E. *Phys. Rev. A* **2003**, *67*, 063405.
15. Helm, H.; Dyer, M. J. *Phys. Rev. A* **1994**, *49*, 2726.
16. Tsubouchi, M.; Suzuki, T. *Phys. Rev. A* **2005**, *72*, 022512.
17. Eppink, A. T. J. B.; Parker, D. H. *Rev. Sci. Instrum.* **1997**, *68*, 3477.
18. Guo, W.; Zhu, J.; Wang, B.; Wang, Y.; Wang, L. *Chem. Phys. Lett.* **2007**, *448*, 173.
19. Vrakking, M. J. J. *Rev. Sci. Instrum.* **2001**, *72*, 4084.
20. Dasch, C. J. *Appl. Opt.* **1992**, *31*, 1146.
21. Becker, A.; Bandrauk, A. D.; Chin, S. L. *Chem. Phys. Lett.* **2001**, *343*, 345.
22. Cremaschi, P.; Chattopadhyay, A.; Madhavan, P. V.; Whitten, J. L. *Chem. Phys.* **1986**, *109*, 117.
23. Edwards, M.; Clark, C. W. *J. Opt. Soc. Am. B* **1996**, *13*, 101.
24. Gibson, G. N.; Freeman, R. R.; McIlrath, T. J.; Muller, H. G. *Phys. Rev. A* **1994**, *49*, 3870.
25. Hansch, P.; Walker, M. A.; Van Woerkom, L. D. *Phys. Rev. A* **1998**, *57*, R709.
26. Sheehy, B.; Dimauro, L. F. *Annu. Rev. Phys. Chem.* **1996**, *47*, 463.
27. Cormier, E.; Garzella, D.; Breger, P.; Agostini, P.; Cheriaux, G.; Leblanc, C. *J. Phys. B* **2001**, *34*, L9.